

Liquid Crystal Visualization in The Study of the Flow in a Shallow Cavity

G.M Zharkova¹, V.N. Kovrizhina², D.S. Mironov³, A.Yu. Pak⁴, A.P. Petrov⁵

Khristianovich Institute of Theoretical and Applied Mechanics SB RAS

¹ ORCID: 0000-0002-0173-2962, zharkova@itam.nsc.ru

² ORCID: 0000-0002-0948-4481, kovrizhina@itam.nsc.ru

³ ORCID: 0000-0001-7316-4282, mironov_ds@itam.nsc.ru

⁴ ORCID: 0009-0004-1947-1651, pak@itam.nsc.ru

⁵ ORCID: 0000-0002-2683-8114, petrov@itam.nsc.ru

Abstract

Using the example of a flow around a shallow cavity, the possibilities of liquid-crystal visualization at subsonic and supersonic flow velocities are demonstrated. To determine the flow structure at the bottom of the cavity, a coating based on a composition of pure cholesteric liquid crystals (ChLC) was used. To determine the distribution of temperatures and heat fluxes, thermosensitive films formed by encapsulation of ChLC in a polymer matrix were used.

Based on the experimental results, the influence of the Mach number on the spatial pattern of the flow inside the cavity and the temperature distribution at the bottom of the cavity was obtained. The pattern of surface streamlines obtained by the LC coating coincides with that obtained using the oil film visualization. In this case, the LC method makes it possible to compare the values of shear stresses in different parts of the surface also. It is found that the occurrence of resonance phenomena leads to restructuring of the flow inside the cavity and a change in the values of shear stresses. It is shown, that in subsonic flow around the zone of increased heat transfer is concentrated near the axis of symmetry of the cavity.

Keywords: liquid crystals, shallow cavity, temperature, shear stress, oil film visualization, Rossiter fluctuations.

1. Introduction

The study of flow in cavities is one of the classical problems of aerodynamics and is of great practical importance in the development of flow control methods, optimization of heat transfer, aerodynamic drag, intensification or attenuation of generated pressure fluctuations. Despite the simplicity of the geometry of a shallow cavity, a complex spatial flow occurs when it flows around. The structure and flow regime in the cavity depend on the ratio of its geometric dimensions [1, 2], the shape/inclination of the walls [3], the velocity and direction of the flow [4 – 6], the thickness and state of the boundary layer at the leading edge [7].

Traditionally, microphones or pressure sensors [2] and hot-wire anemometers [8] are used to study such flows. In the study of thermal processes on the surface of the model, thermocouples are used. [3]. Among the panoramic methods for flow investigations, infrared thermography (IRT), oil film methods, the method of sublimation coatings, etc. can be used. When studying complex flows, a combination of various panoramic imaging methods is effective, the comparison of which makes it possible to increase the reliability of experimental data, especially given the relatively few works devoted to the diagnosis of heat transfer and surface friction in cavities.

For a more detailed study of thermal processes inside the cavity, liquid crystal (LC) coatings are of particular interest [9 – 14]. This is due to the possibility of obtaining pano-

ramic qualitative and quantitative data on temperature, heat flux and their evolution over time. In addition, LC coatings that are sensitive to tangential stress allow you to visualize the picture of the limiting stream lines and the distribution of tangential stresses.

The purpose of this work is to test LC methods for visualizing the panoramic distribution of temperature and surface shear stress using the example of a shallow cavity.

2. Fundamentals of liquid crystal visualization

The main features of liquid crystals (LC) are the high lability of their structure and anisotropy of physical properties. As a consequence, small external disturbances (temperature, mechanical stresses, electric and magnetic fields) cause their deformation, which leads to a change in the orientation of molecules in the layer, their supramolecular structure and optical properties.

The methods of LC visualization are based on the diffraction of light on the spiral structure of one of the types of LC – cholesteric LC (ChLC) [15]. Being applied on the surface, this type of LC can form 2 textures: confocal and planar. The confocal texture is characterized by a disorderly arrangement of the optical axes of the cholesteric spiral, and in the planar texture all the axes of the spirals are oriented in the same direction and perpendicular to the surface on which the coating is applied (Fig.1).

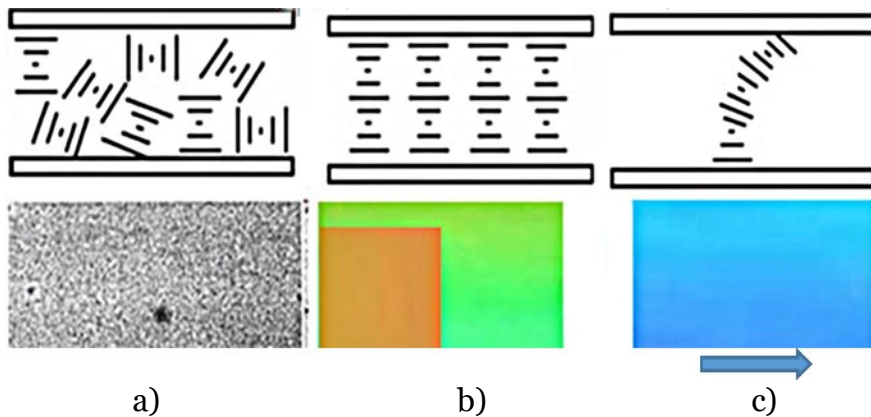


Fig. 1. The structure of the ChLC (upper row) and the optical response of the LC: (a) confocal texture; (b) planar texture; (c) planar texture deformed by tangential shear.

The white light incident on a planar texture is reflected selectively in accordance with the Wolf-Bragg condition: the wavelength of the selective reflection maximum $\lambda_o = 2nd \sin \theta$, where n is the average refractive index of light, $d = P/2$ is the pitch (the period of the diffraction grating), and θ is the angle between the incident beam and the cholesteric plane. For the real case with an imperfect planar texture, λ_o also depends on the angles of incidence φ_n and light reflection φ_o :

$$\lambda = Pn \cos \frac{1}{2} \left[\arcsin \left(\frac{\sin \varphi_n}{n} \right) + \arcsin \left(\frac{\sin \varphi_o}{n} \right) \right]$$

In aerodynamic experiments, the temperature, mechanical shear, and pressure simultaneously affect the ChLC. At the same time, under the conditions of our experiment, the influence of pressure can be neglected, since LCs change their properties only when they are exposed to pressure above 10 atm.

In ITAM SB RAS (Khristianovich Institute of Theoretical and Applied Mechanics, Siberian Branch of Russian Academy of Science), the coatings based on cholesterol ethers and a number of acids have been developed and applied, their wavelength of selective reflection changes both under the influence of the temperature of the surface under study (i.e. the pitch), and under the influence of deformation induced by a mechanical shear (i.e., the an-

gle of inclination of the spiral optical axis). Figures 2 and 3 show color-temperature dependences of various mixtures of cholesterol esters.

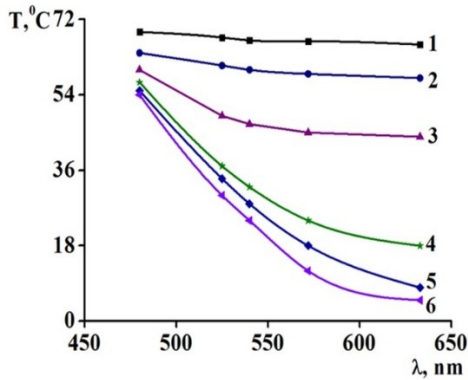


Fig.2. An example of color-temperature dependences of LC compositions with different temperature sensitivities.

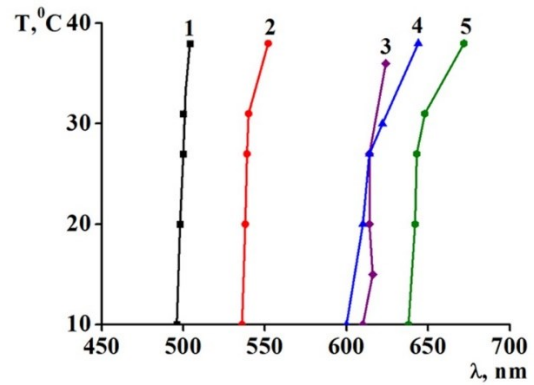


Fig.3. An example of color-temperature dependences of LC compositions insensitive to temperature.

To protect thermosensitive compounds from the influence of mechanical shear, they are encapsulated in a polymer matrix. As a result, thermo-indicating films are obtained that are sensitive only to temperature (Fig. 4 and 5).

The main characteristics of the developed LC films are: the thickness is 20÷50 microns; the temperature range is from -5 to 150 C; the temperature sensitivity is 10^{-4} w/cm²; the response time 3÷30 ms; the life time is above one year.

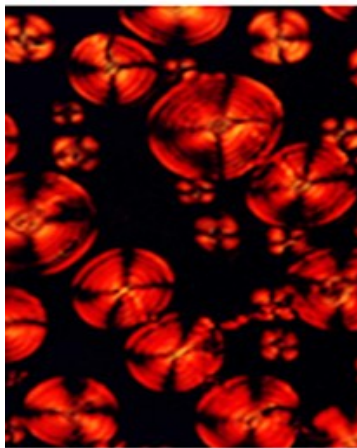


Fig.4 Microscopic structure of polymer-liquid crystal film.

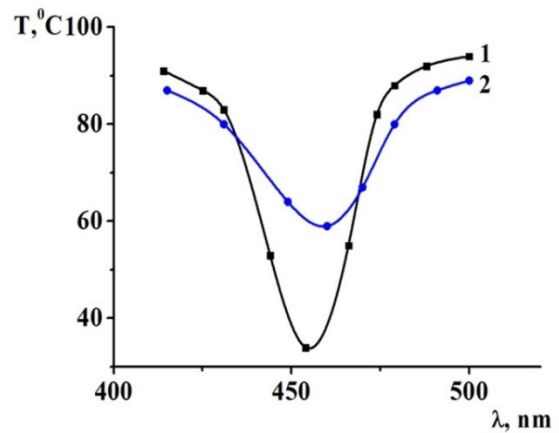


Fig.5. Reflection spectrum of pure LC (1) and LC in polymer (2).

Chromatic coordinates in a different color coordinate system are used as color characteristics of the optical response of the LC to a particular effect and for digital processing of color images obtained in the experiment. As a rule, the conversion of the color coordinate system from the RGB system to the HSI system (hue, saturation, intensity) is used.

In our experiments, we used the chromatic coordinate – H (Hue). As the local temperature decreases, the LC coatings monotonously change their color from blue to red. Fig. 6 shows a typical dependence of the Hue on the temperature $H(T)$. The dependence of the hue on the tangential stress in the conditions of an experiment with a coating based on a mixture of pure cholesteric LC is also described by a polynomial of a low degree. Therefore, for a qualitative analysis of the flow structure on the model under study, it is convenient to use Hue maps [16].

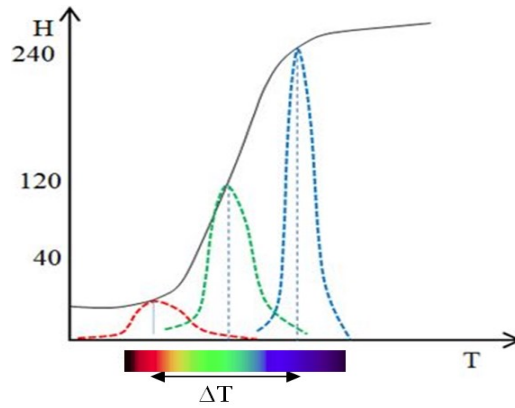


Fig. 6. Typical dependence of hue on temperature $H(T)$.

The qualitative interpretation of the obtained LC thermogramm is based on the correlation of flow characteristics with heat transfer, such as: the area of flow attachment corresponds to increased heat transfer from the surface (relatively cold areas are red), stagnant areas correspond to the reduced heat transfer (relatively hot blue areas of the surface), etc. Similarly, under the influence of skin friction in areas with a higher level of tangential stresses, the wavelength of the reflected light is shifted to the blue region of the spectrum. In the areas of separation, the color of the coating remains the original. The hue of the LC optical response is used for calibration and development of LC compositions with the required metrological characteristics.

3. Experimental conditions

The experiments were carried out in a wind tunnel T-325M ITAM SB RAS with a cross section of the test section $40 \times 40 \text{ mm}^2$, which is blow-down type facility. A set of replaceable test sections is available to simulate different speeds of the incoming flow. The subsonic test section has a constant cross section and a retaining shutter at the outlet, which allows you to smoothly change the inflow Mach number from 0.3 to 0.7. Supersonic test sections have a built-in nozzle for a certain Mach number (2, 3, or 4). The Reynolds number can be changed by changing the total pressure in the wind tunnel pre-chamber. The Reynolds unit number was $Re_1 = 19 \cdot 10^6 \text{ m}^{-1}$ in all experiments conducted, except for experiments with a maximum velocity of $M = 4$, where $Re_1 = 21 \cdot 10^6 \text{ m}^{-1}$.

A model of a plate with a rectangular cavity was made of fiberglass and installed in one of the replaceable side walls of the test section. In the experiments, a cavity with a length of $L = 60 \text{ mm}$, a width of $W = 30 \text{ mm}$ and a depth of $D = 9 \text{ mm}$ was used. A cavity with such a size ratio belongs to the so-called shallow cavity [2], when the ratio of length to depth L/D is greater than one, and the flow realized in it at $L/D = 6.7$ belongs to the open type.

Visual access to the test section of the wind tunnel was provided by a window with optical glass on the side wall opposite the cavity. Outside the wind tunnel there was a lighting system and a camera. Fig. 7 presents the experimental scheme and the coordinate system.

To control the level of pressure fluctuations and determine the flow mode in the upper wall of the test section in the section $x/L = 1.17$ (see Fig. 1 b), a Kulite pressure sensor XCS-093-25A was installed. To determine the structure of the flow in the cavity, an oil-black visualization was used, which allows to obtain streamlines on the model surface. For this purpose, a mixture of spindle oil with soot was used. For better visibility of the streamlines, the cavity model was painted white. The holding time of the oil-soot mixture in the flow was determined empirically by recording video for each of the flow regimes.

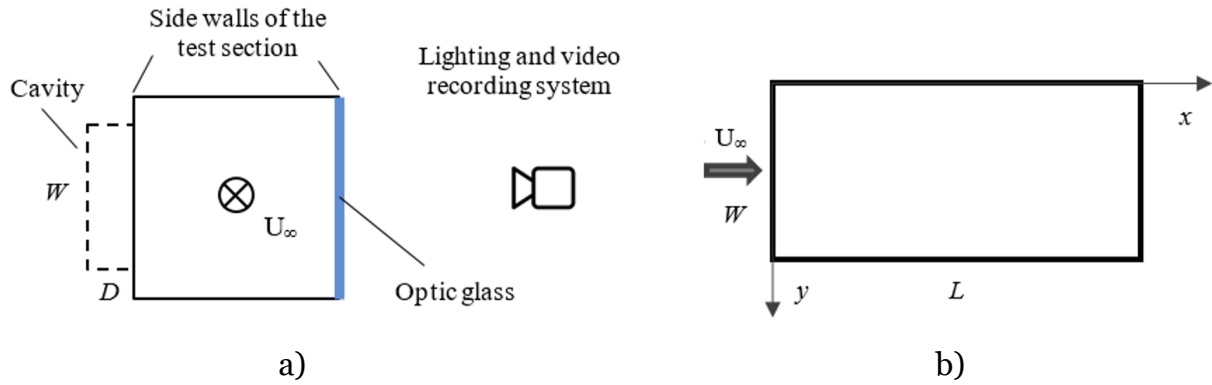


Fig. 7. The experimental scheme (front view) (a) and the coordinate system used in the cavity (b)

In order to verify the data on the structure of the flow in the cavity obtained with the help of oil-film visualization and to study the influence of the Mach number on it by methods of liquid crystal coatings, diagnostics of temperature fields was performed. The duration of the experiment was also controlled during video recording (25 frames per second) and was no more than 100, sometimes 200 seconds, which allowed us to neglect heat overflows according to the model under study. The methods of application, calibration and digital processing of experimental data obtained using LC are described, for example, in [9 – 15].

Two types of LC coatings were used in the work: a temperature-sensitive polymer-liquid crystal film and a coating based on a composition of pure cholesterol LCD (CLC) sensitive to the tangential stress of surface friction.

The thermosensitive film with the bandwidth of the selective reflection region $\Delta T = (15 \div 17)^\circ\text{C}$ was stuck to the model. Pure LCs, sensitive to the tangential stress and insensitive to temperature in the temperature range under study, were applied to the model by spraying, followed by the creation of a selectively reflecting light planar texture of the ChLC before each experiment, if necessary. The response time of the LC is 20 – 100 ms, depending on the composition viscosity.

Prior to the experiment, the cavity model, coated with a thermosensitive film, had a dark blue color at the room temperature. After switching on the flow, due to cooling, the color of the LC coating changed in accordance with the local intensity of heat exchange of the surface with the flow. As the local temperature decreases, the coatings monotonically change their color from blue to red. At the same time, the hue H decreases almost linearly.

4. Results and discussion

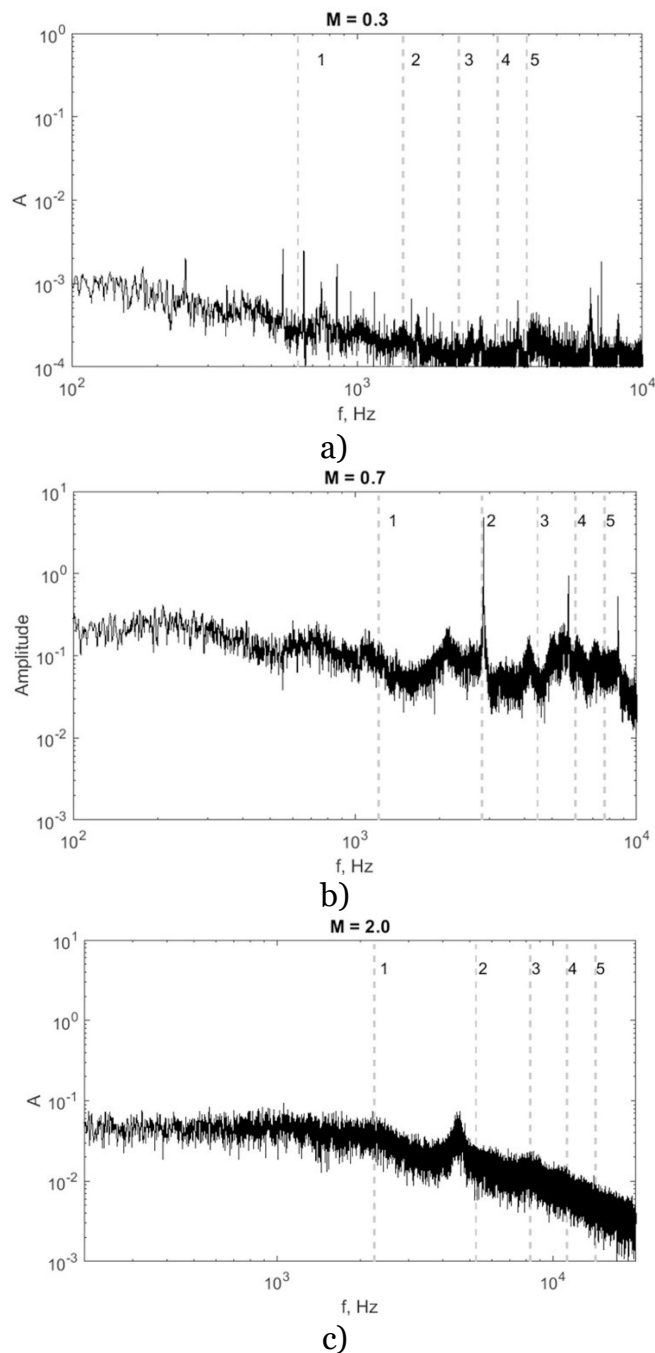
Previously, it was found that in the studied shallow cavity at Mach numbers from 0.3 to 0.75, two types of flow structure can be realized, which correlate with the absence or presence of generation of high-intensity acoustic fluctuations, called the Rossiter fluctuations [17, 18] (Fig.8). To determine the frequencies of individual fluctuation modes, the Rossiter formula is derived.

$$f = \frac{U_\infty}{L} \frac{m - \alpha}{M + 1/k}$$

where U_∞ is the free stream velocity, m is the mode number, $k = U_c/U_\infty$ is the dimensionless vortex drift velocity, α is the phase delay (in wavelengths, $\alpha < 1$) as a result of the time delay between the moment of collision of the vortex with the trailing edge of the cavity and the moment of emission of the sound wave. The values of the empirical constants $k = 0.57$ and $\alpha = 0.25$ correspond most exactly to the majority of experimental data [19, 20].

Figure 8 shows examples of the signal spectra of the pressure sensor installed on the side of the cavity under study. The dotted lines on them indicate the frequencies calculated by formula (1), with the indication of the number of the corresponding mode. The spectrum corresponding to a Mach number of 0.3 shows several discrete peaks close in frequency to the first Rossiter mode. On the spectrum corresponding to $M = 0.7$, a discrete peak of significant amplitude is observed at a frequency coinciding with the second Rossiter mode, which indicates the occurrence of resonant phenomena in this flow regime.

At supersonic flow velocities, pressure fluctuations close in frequency to Rossiter fluctuations are observed only at $M = 2$. A noticeable difference from the calculated value of the second mode may be due to the fact that the same values of the empirical constants k and α in formula (1) were used for the calculation, as for subsonic velocities of the oncoming flow.



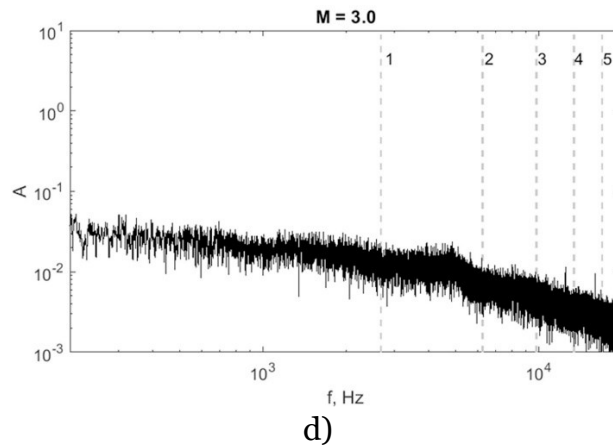


Fig.8. Fourier spectra of the pressure sensor signal.

The first type of flow, when there are no high-intensity fluctuations, is observed at Mach numbers up to 0.4 and at $M = 0.6$. The structure of such a flow on the example of $M = 0.3$ is shown in Fig. 9a. Here and further, the freestream is directed from left to right. There is a stagnant zone in the front part of the cavity, occupying about 25% of the length of the cavity. The flow has a cellular, slightly asymmetrical structure, which may be due to the non-strict perpendicularity of the leading edge to the velocity vector of the incoming flow or errors in the manufacture of the model. The reversal flow in the middle part of the cavity indicates the presence of two main vortices inside the cavity, swirled by the flow. The absence of shear layer attachment to the bottom also indicates the implementation of an open type of flow. The attachment line is in position $x/L = 0.85$.

When high-intensity fluctuations occur, a noticeable restructuring of the flow occurs. These types of flow correspond to the Mach numbers equal to 0.5 and above 0.65. The flow structure at $M = 0.7$ is shown in Fig. 9b. In such cases, attachment points (sources) arise at the bottom, from which a comprehensive spreading occurs. The streamlines from these sources, diverging first in all directions, are carried away by the return flow to the front wall of the cavity. This structure of the streamlines indicates the formation of toroidal vortices elongated towards the leading edge. In addition, the reattachment line is shifted closer to the rear wall up to the position $x/L = 0.9$.

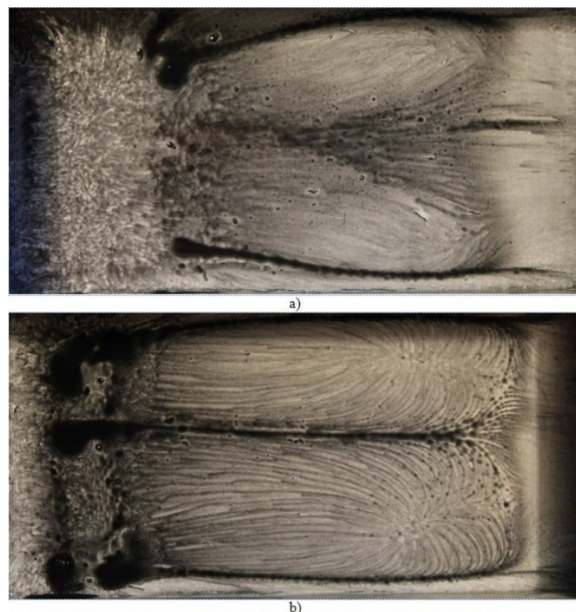


Fig.9. Flow structure on the cavity bottom. Oil-film visualization $M=0.3$ (a) and $M=0.7$ (b)

Similar structures are also visualized by the method of an LC coating sensitive to the surface shear stress (Fig. 10-11).

In addition to the qualitative determination of the direction of the streamlines, unlike oil-film visualization, these images show a change in the LC coating color. Under the influence of shear in areas with a higher level of tangential stresses, the wavelength of the reflected light is shifted to the blue region of the spectrum. In the areas of separation, the color of the coating remains the original. A more pronounced change in the color of the LC coatings at Mach numbers of 0.7 and 2 can be noted. This may be due to an increase in the shear stress due to the presence of high-intensity fluctuations of the flow parameters inside the cavity.

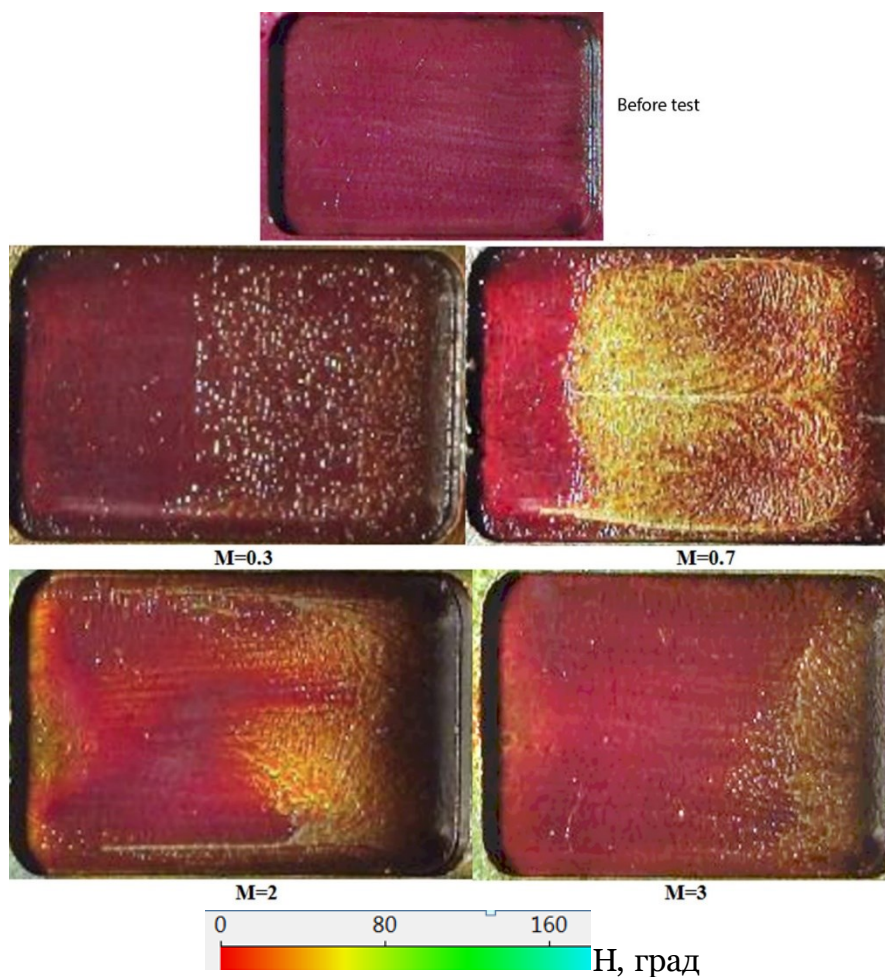


Fig.10. Flow structure on the cavity bottom. LC coating

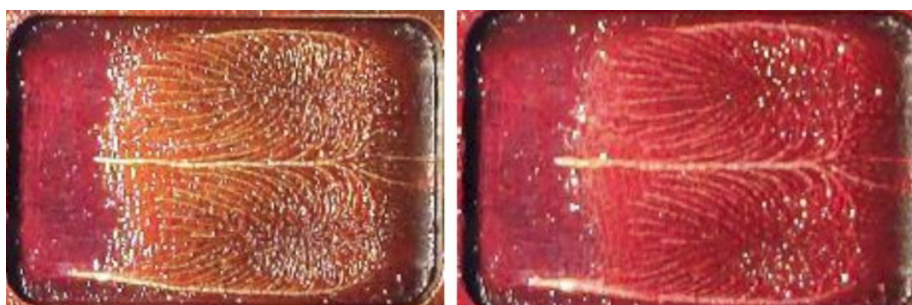


Fig. 11. Picture of the streamlines in 60 and 80 s after the flow was turned off. $M=0.7$

At $M = 2$, the three-dimensional flow pattern in the cavity became noticeably asymmetric, the observed size of the stagnant region increased compared to subsonic flow velocities. The yellow color of the LC coating in the spreading zone indicates a lower level of

tangential stresses at such a flow velocity than at $M = 0.7$. The information obtained using the LC permits optimally switching to local instrumental measurements on the surface under study (thermocouples, surface sensors).

It should be noted that the change in the distance from the nozzle of the test section to the cavity, i.e. the thickness of the boundary layer at the leading edge (within the framework of this experiment) does not affect the flow structure (Fig. 12).

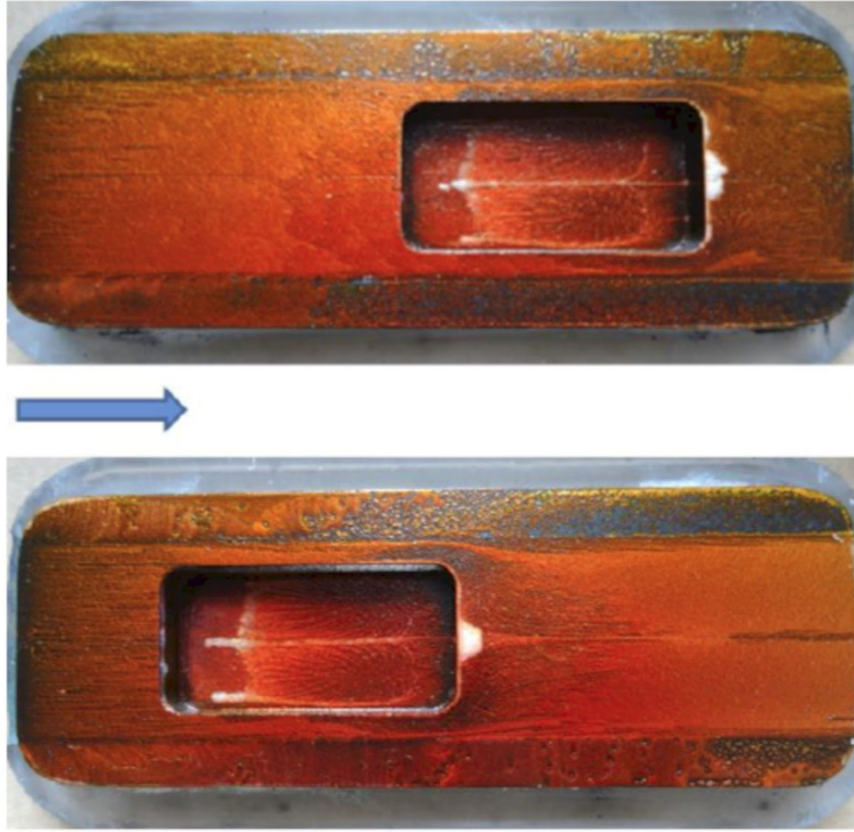


Fig. 12. Influence of the distance to the cavity on the flow pattern ($M = 0.7$)

Let us now consider the results obtained by the method of thermosensitive LC coatings with a nominal sensitivity range of $\Delta T = 15 \div 17^\circ \text{C}$. Figure 13 shows the time dependence of the optical response of the LC during a start-up lasting about 90 seconds at $M = 2$. The red areas correspond to increased heat transfer from the surface to the gas, respectively, the blue areas correspond to reduced heat transfer. Despite the fact that the temperature difference during the experiment on the surface of the plate is slightly larger than the dynamic range of the LC used ($\Delta T = 2^\circ \text{C}$) and visually not the entire surface of the plate is painted at the same time, the temperature imprint of the flow structure of the supersonic flow on the plate and in the cavity was obtained. Hue maps also show that this range of operating temperatures of the LC allows you to almost completely obtain the distribution of instantaneous temperature in the cavity.

As is known, having a local temperature dependence on time $T(x, y, t)$ under certain boundary conditions on the surface, it is also possible to obtain the heat flux density.

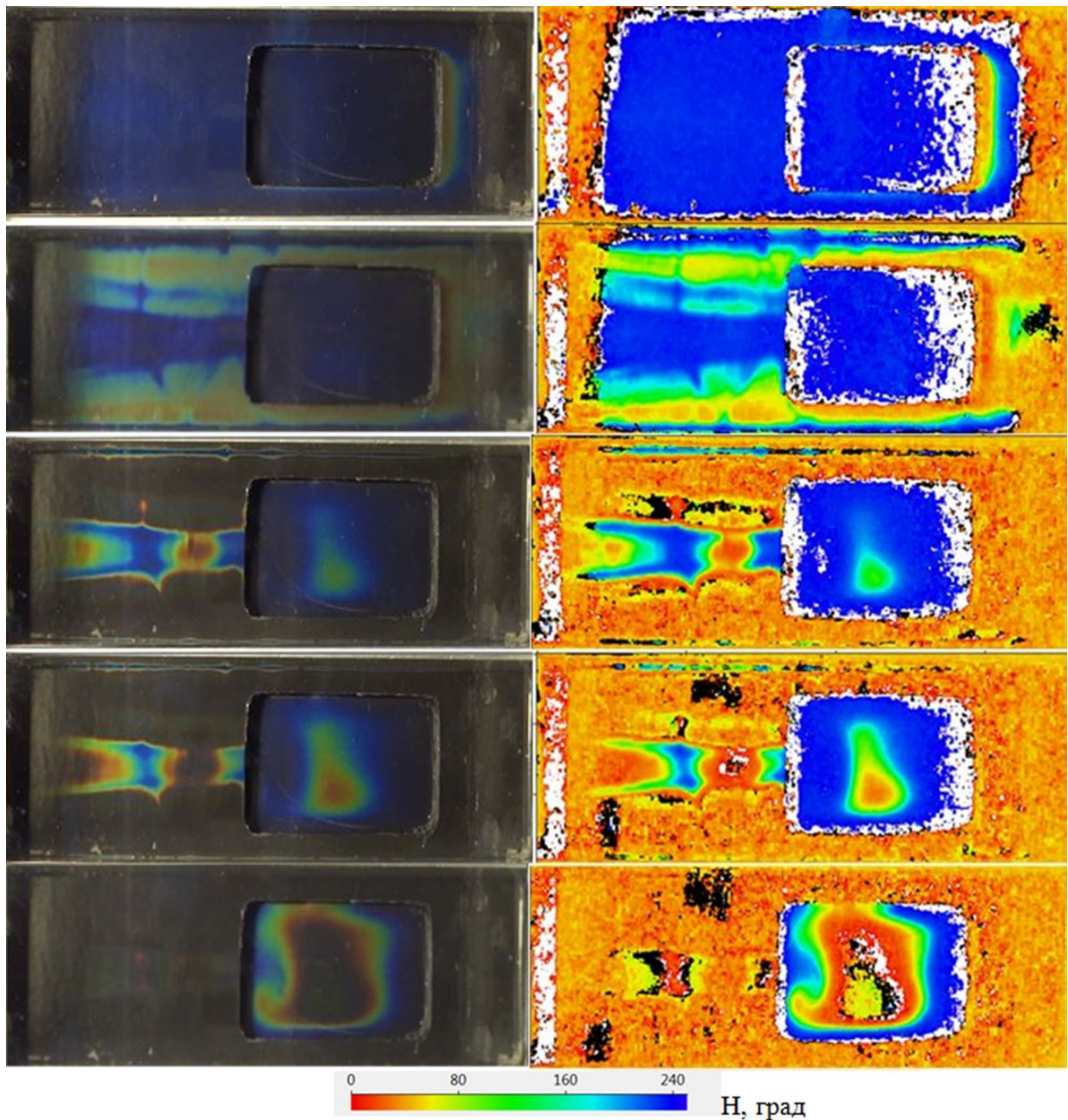


Fig. 13. Change of LC thermographs during the experiment (from top to bottom) at $M = 2$ (left) and corresponding hue maps (right).

Fig. 14 shows the LC visualization of the temperature field and the Hue map at Mach numbers: 0.7, 2 and 3. It can be seen that the maximum heat transfer at $M = 3$ occurs in the regions corresponding to the centers of the spreading areas (see Fig. 11b), despite the absence of resonance at $M = 3$. In these positions, the cooling is maximum and the model has a red color. At the same time, at the subsonic velocity of the incoming flow ($M = 0.7$), only one region of increased heat transfer is observed near the center of the cavity, corresponding to the region of increased values of tangential stresses (see Fig. 4b). This may be due to the redistribution of mass flow at the cavity bottom due to an increase in velocity and a decrease in flow density, owing to the intensification of heat exchange near the rear wall due to an increase in the level of fluctuations generated at the rear edge by a faster mixing layer.

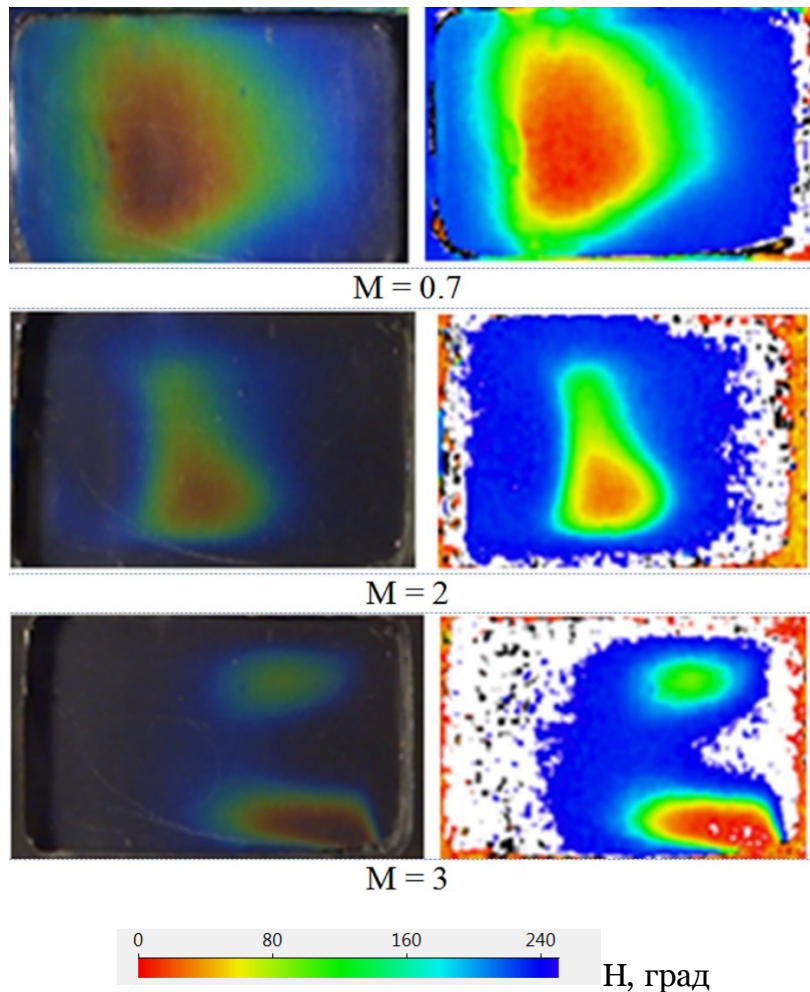


Fig. 14. LC visualization of the temperature field (left) and hue maps at different Mach numbers (right)

5. Conclusions

The paper presents the results of testing two types of LC coatings (sensitive to temperature or shear stress) and methods of their application to visualize the panoramic distribution of these parameters on the example of a flow in a shallow cavity.

The use of coatings based on pure LCs makes it possible to obtain surface streamlines similarly to the oil-film visualization method, while additionally it is possible to qualitatively compare the values of shear stresses in different parts of the model.

Both types of LC coatings made it possible to detect the features of the topology of the near-wall subsonic flow on the surface under study, as well as the structure of the supersonic jet and its shape on the surface of the model as a function of time. In addition to topology, the method of thermosensitive LC films makes it possible to study heat transfer, which is relevant when used in a number of technological processes.

The results of visualization of temperature fields showed that at subsonic freestream velocities, the maximum heat transfer takes place in the middle part of the cavity, where the near-wall flow velocity is maximum. At supersonic speeds, the areas of maximum heat transfer correspond to the reattachment zones.

Acknowledgements

The work was carried out on the topic of the state task (state registration number 121030500158-0).

References

1. **Disimile P., Toy N., Savory E.** Effect of planform aspect ratio on flow oscillations in rectangular cavities // *Journal of Fluids Engineering-transactions of The Asme - J. FLUID ENG.* 2000. Vol. 122. DOI:10.1115/1.483223.
2. **Mendoza J., Ahuja K.** Effects of cavity dimensions, boundary Layer, and temperature on cavity noise with emphasis on benchmark data to validate computational aeroacoustic codes. 1995. 261 p.
3. **Dyachenko A.Yu., Terechov V.I., Yarygina N.I.** Obtekanie turbulentnym potokom poperechnoi kaverny s naklonnymi bokovymi stenkami. 2.Teploobmen.// *Prikladnaya mekhanika i texnicheskaya phisika.* 2007. Tom 48, № 4, C.23-29.(In Russian)
4. **Savory E., Toy N., Okamoto S., Yamanishi Y.** The internal flow field associated with yawed three-dimensional rectangular cavities // *Journal of Flow Visualization and Image Processing.* 2000. Vol. 7. № 3. P. 217-229.
5. **Czech M., Savory E., Toy N., Mavrides T.** Flow regimes associated with yawed rectangular cavities // *The Aeronautical Journal.* Cambridge University Press, 2001. Vol. 105. № 1045. P. 125-134.
6. **Mironov D.S.** Experimental investigation of pressure fluctuations generated by a shallow open cavity using time-frequency methods of data processing // *Thermophysics and Aeromechanics.* 2011. Vol. 18. № 3. C. 385-395.
7. **Grace M.S., Dewar W.G., E. Wroblewski D.** Experimental investigation of the flow characteristics within a shallow wall cavity for both laminar and turbulent upstream boundary layers // *Experiments in Fluids.* 2004. Vol. 36. № 5. P. 791-804.
8. **Mironov D.S.** The emergence of resonance in the transonic flow of a shallow three-dimensional cavity // *XI All-Russian Congress on fundamental problems of theoretical and applied mechanics: proceedings.* Kazan, 2015. pp. 2568-2570.
9. **Zharkova G.M., Kovrizhina V.N.** Panoramic diagnostics of surface temperatures and heat flux cholester in an aerodynamic experiment // *Engineering Physics Journal.* 2010. Vol. 83. № 6. C. 1072-1083.
10. **Zharkova G.M., Kovrizhina V.N., Petrov A.P., Podyachev S.P.** Panoramic diagnostics of tangential stresses on the channel wall with a protrusion using liquid crystals // *Thermophysics and aeromechanics.* 2016. No.6. pp. 865-873.
11. **Zharkova G.M., Kovrizhina V.N., Petrov A.P., Mosharov V.E., Radchenko V.N., Shapoval E.S.** On the use of liquid crystals to visualize the structure of wall flow in experimental aerodynamics // *Results of fundamental research in applied problems of aircraft engineering. Collection of articles.* Moscow: Russian Academy of Sciences ("Science" of the Russian Academy of Sciences). 2016. pp. 113-125. ISBN 978-5-9908169-6-1.
13. **Zharkova G.M., Kovrizhina V.N., Petrov A.P.** Panoramic temperature, pressure, and shear stress sensors based on liquid crystal composites // *Polymer Science, Series C.* 2018. Vol. 60. No. 1. P. 14-22.
14. **Zharkova G.M., Kovrizhina V.N.** Mechano-optical effects in liquid crystals and their use for measuring tangential stresses in an aerodynamic experiment // *Liquid crystals and their practical use.* 2022. Vol.22. No.3. pp. 5-14.
15. **Belyakov, Sonin A.S.** Optics of cholesterol liquid crystals. M.: Nauka, 1982. 360 p.
16. **Zharkova G.M., Kovrizhina V.N., Podyachev S.P.** Analysis and interpretation of video recording data of experiments with LCDD coatings // *Scientific visualization.* 2017. Vol. 9. No. 3. pp. 96-102.
17. **Mironov D.S., Lebiga V.A., Zharkova G.M., Kovrizhina V.N., Petrov A.P.** Investigation of flow features in a rectangular cavity using panoramic visualization methods // *AIP Conference Proceedings.* 2023. V. 2504. No. 030036. (doi: 10.1063/5.0132807).

18. **Rossiter J.E.** Wind-Tunnel Experiments on the Flow over Rectangular Cavities at Subsonic and Transonic Speeds. 1964.
19. **Heller, H.H., Bliss, D.B.** The Physical Mechanism of Flow-Induced Pressure Fluctuations in Cavities and Concepts for Their Suppression // AIAA Paper 75-0491. 1975.
20. **Ahuja, K.K., Mendoza, J.** Effects of Cavity Dimensions, Boundary Layer and Temperature on Cavity Noise With Emphasis on Benchmark Data To Validate Computational Aeroacoustic Codes // CR 4653. National Aeronautics and Space Administration. 1995.